Qualification of Boron Carbide Ceramics for Use in ITER Ports

Andrey Shoshin, Alexander Burdakov, Maxim Ivantsivskiy, Sergey Polosatkin, Maria Klimenko, Alexey Semenov, Sergey Taskaev, Dmitrii Kasatov, Ivan Shchudlo, Alexander Makarov, and Nikolay Davydov

***Abstract*— Boron carbide has been proposed for the neutron protection of equipment in the ITER diagnostic ports and for reducing the dose to maintenance personnel. The chemical composition, vacuum, and thermal properties of ceramics of boron carbide were studied. It is demonstrated that the outgassing rate of ceramics meets the requirements of the ITER Vacuum Handbook. Calculation of the total gas emission from the ITER equatorial port #11 is carried out. The contact thermal conductivity at the boundary between ceramics and bronze is measured. Manganese content is determined by the method of activation analysis in ceramics. It is shown that sintered and hot-pressed boron carbide ceramics can be used in the ITER diagnostic ports.**

***Index Terms*— Boron carbide ceramic material properties, ITER port mechanical engineering.**

I. Introduction

ONE of the functions of ITER diagnostic port-plugs is neutron protection of the equipment installed in the port, as well as reducing the radiation background in the area of reactor elements periodically requiring access to maintenance personnel. The Budker Institute of Nuclear Physics (BINP) is an integrator of ITER diagnostic ports (equatorial port #11, upper ports #02, 07, and 08). The BINP has extensive experience in the study of materials for fusion facilities using various technologies [1], including electron [2]–[4] and proton [5]–[7] accelerators, synchrotron radiation [8], [9], and theoretical modeling [10], [11].

Manuscript received July 10, 2019; revised August 9, 2019; accepted August 22, 2019. This work was supported in part by the Institution "Project Center ITER" (Rosatom) under Contract 17706413348180000850/18-07 and in part by the Russian Science Foundation under Project 19-72-30005. The review of this article was arranged by Senior Editor G. H. Neilson. *(Corresponding author: Andrey Shoshin.)*

A. Shoshin, S. Taskaev, and D. Kasatov are with the Budker Institute of Nuclear Physics, Siberian Branch of the Russian Academy of Sciences, 630090 Novosibirsk, Russia, and also with the Physics Department, Novosibirsk State University, 630090 Novosibirsk, Russia (e-mail: shoshin@inp.nsk.su).

A. Burdakov, M. Ivantsivskiy, S. Polosatkin, M. Klimenko, and A. Semenov are with the Budker Institute of Nuclear Physics, Siberian Branch of the Russian Academy of Sciences, 630090 Novosibirsk, Russia, and also with the Physics and Technical Department, Novosibirsk State Technical University, 630092 Novosibirsk, Russia (e-mail: s.v.polosatkin@inp.nsk.su).

I. Shchudlo and A. Makarov are with the Budker Institute of Nuclear Physics, Siberian Branch of the Russian Academy of Sciences, 630090 Novosibirsk, Russia (e-mail: a.n.makarov@inp.nsk.su).

N. Davydov is with the Physics Department, Novosibirsk State University, 630090 Novosibirsk, Russia (e-mail: davnvl2000@gmail.com).

Color versions of one or more of the figures in this article are available online at http://ieeexplore.ieee.org.

Digital Object Identifier 10.1109/TPS.2019.2937605

At the stage of conceptual design in diagnostic ports, it was not supposed to use ceramics. The strict restriction on the total weight of the port does not allow filling the entire port with metal. The cavities inside the port, together with the straight vacuum tubes of the diagnostic systems, make it impossible to provide the required attenuation parameters to protect the diagnostic detectors and to provide the shutdown dose rate that would allow workers to service the diagnostics. Also, the peculiarities of the French nuclear regulation do not allow using water (as a neutron decelerator) in large quantities in ports.

For this reason, it was suggested that other materials be used in ports, primarily boron carbide. Due to the low atomic weight and the high absorption cross section of thermal neutrons, boron carbide can serve as an effective flux attenuator for both fast and thermal neutrons. Initially, it was proposed to use boron carbide powder in closed volumes. However, this is contrary to the ITER vacuum rules. Therefore, the task arose to confirm that boron carbide ceramics could be used openly in ITER ports.

Properties of ceramics based on boron carbide strongly depend on its manufacture technology. Boron carbide ceramics has a density of $2.36-2.37$ g/cm^3 for sintered ceramics and $2.51-2.52$ g/cm^3 for hot-pressed ceramics. The density difference is only 6%. This article did not consider the heavier (due to the admixture of silicon) reaction bonded ceramics, their properties are presented in [1].

Manufacturers have extensive experience in the production of this material, as one of the broad applications of hot-pressed ceramic is bullet-proof shells. In Russia, there are several manufacturers: Virial, Ltd. (St. Petersburg, http://www.virial.ru), NEVZ-Ceramics (Novosibirsk, http://www.en.nevz.ru), and Beeforce (Tver', http://www.ekzivent.ru/).

For the possible use of boron carbide in ITER ports, it is necessary to confirm its suitability for use in vacuum and under neutron loads, i.e., the ceramic should not contain dangerous contaminants and shall meet the requirements of the ITER Vacuum Handbook (IVH) [12]. In July 2017, limited use of boron carbide in the ITER vacuum chamber was allowed. However, ITER still does not have an approved specification for any type of boron carbide ceramic.

II. Chemical Composition and SEM Images

Previously, measurements were made of the chemical composition of different types of ceramics from different

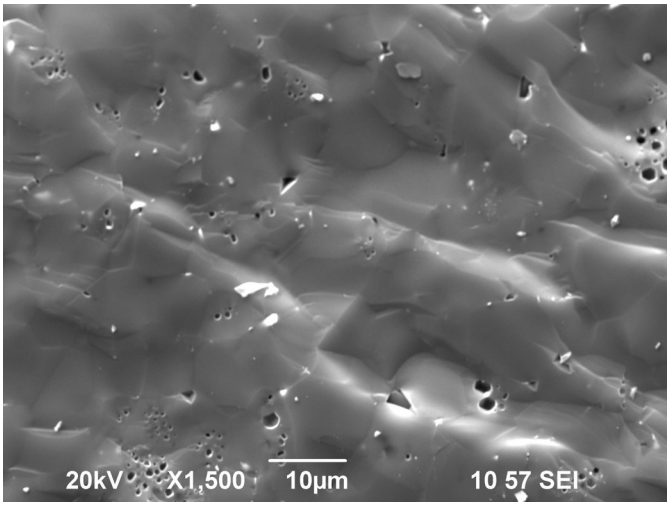

Fig. 1. SEM images of the hot-pressed ceramic fracture (type 50-18 produced by Beeforce).

manufacturers [1]. The amount of impurities in sintered and hot-pressed ceramics of boron carbide did not exceed 1%, which meets the requirements of ITER [1]. Recently, similar studies have been carried out on two other types of hot-pressed ceramics (types 50-18 and 51-18) produced by Beefors. Also, hot-pressed ceramics of other types and other manufacturers [1] have a small amount of micrometer pores in them (Fig. 1).

The chemical composition was also similar to that of other types of hot-pressed ceramics [1]. Ceramic types 50-18 and 51-18 contain the following admixtures: Fe 0.12−0.24%, O 0.13−0.16%, Si 0.07−0.09%, Al 0−0.05%, and Cr 0−0.03%.

III. Sintered Ceramic Outgassing Test

The outgassing tests have been carried out to confirm that boron carbide ceramics can be used in the ITER vacuum chamber and meet the IVH requirements [12], i.e., the outgassing rate is not more than 1×10^{-7} Pa·m^3·s^{-1}·m^{-2} for hydrogen and not more than 1×10^{-9} Pa·m^3·s^{-1}·m^{-2} for all other impurities. Previously, data on the outgassing rate of hot-pressed ceramics and preliminary data on sintered ceramics were obtained [1]. The measurements showed that the outgassing rate for the hot-pressed ceramic produced by Virial was 1.0×10^{-8} Pa·m^3·s^{-1}·m^{-2}, so this ceramic meets the requirements of the IVH [1]. Preliminary experiments with a small amount (20 samples) of sintered ceramics produced by Virial have an estimated outgassing rate of 9.1×10^{-8} Pa·m^3·s^{-1}·m^{-2} [1]. In order to obtain reliable data, new tests were carried out with a large number of sintered ceramics. We used 638 samples of $55 \times 55 \times 5$ mm in size, with a total area of 4.56 m^2 (Fig. 2).

In January 2019, a meeting was held with the ITER vacuum group and the test procedure was modified, upon their recommendation, from the tests in [1]. In particular, the maximum heating temperature before measurements was reduced to 240 °C to make the tests more realistically simulate the baking conditions in the ITER port.

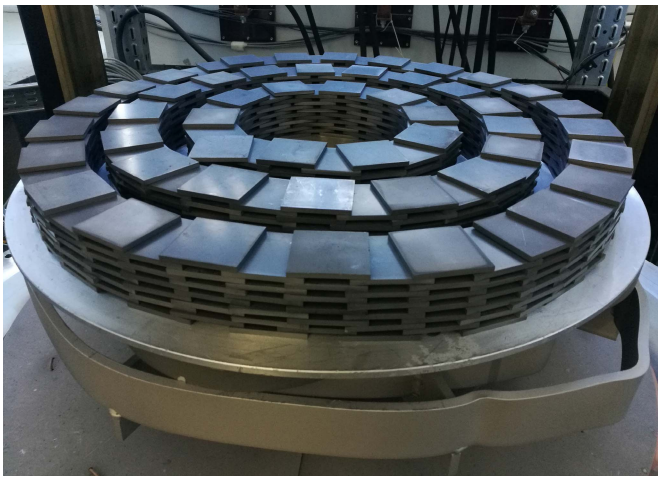

Fig. 2. 638 bars of $55 \times 55 \times 5$ mm sintered ceramic after annealing in a vacuum furnace before outgassing testing. Ceramics produced by Virial. Total surface area of samples is 4.56 m^2.

TABLE I
Outgassing Rate of Virial-Made Sintered Ceramics

Time after heating up to 100 °C	Outgassing Rate, Pa·m^3·s^{-1}·m^{-2}
5 h	1.04E-08
24 h	1.00E-08
29 h	9.96E-09

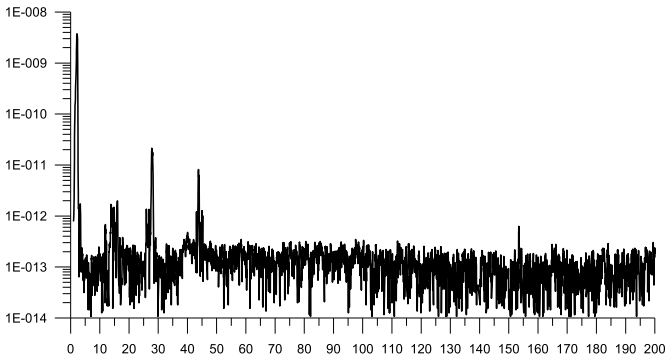

Fig. 3. RGA scan for Virial-sintered boron carbide after 24 h at 100 °C.

To prepare for conducting measurements, the sample was cleaned with ethyl alcohol and in an ultrasonically agitated bath of distilled water, baked at 1000 °C in vacuum prior to testing (Fig. 2).

Vacuum Test Procedure:

1) Ramp up from room temperature to 200 °C: 10 h.
2) Steady temperature at 200 °C for 11 h.
3) Ramp up to 240 °C: 1 h.
4) Steady temperature at 240 °C for 24 h.
5) Cool down to room temperature: 18 h.
6) Ramp up to 100 °C: 3 h.
7) Steady temperature at 100 °C for testing.

After reaching a temperature of 100 °C, measurements were made in 5, 24, and 29 h to demonstrate a reduction in gas emission (Table I). Residual gas analyzer (RGA) scans are shown in Figs. 3 and 4. According to ITER requirements,

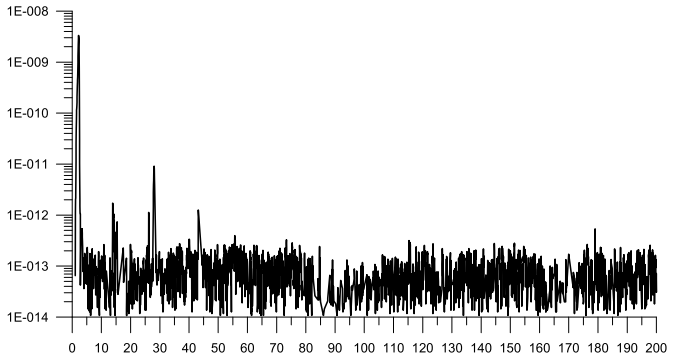

Fig. 4. RGA scan for Virial-sintered boron carbide after 29 h at 100 °C.

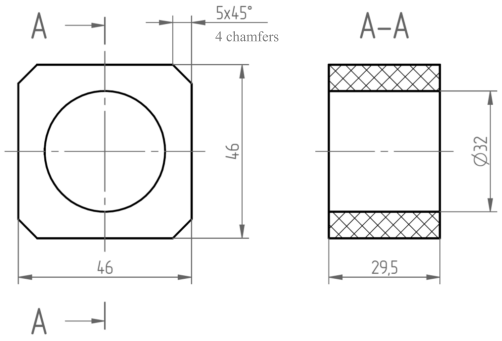

Fig. 5. Design of B_4C blocks for ITER Equatorial port #11 FDR.

the value of impurity peaks in the spectrum should be at least 100 times lower than the hydrogen peak. In Figs. 3 and 4, this requirement is met with a large reserve. In 24 h, the outgassing rate of the B_4C samples at 100 °C decreased by 4% (Table I). Thus, the vacuum properties of sintered and hot-pressed ceramics produced by Virial were the same, and both types of ceramics meet the requirements of ITER. Since sintered ceramics are cheaper and can be produced in large quantities, it is likely that it will be used in the equatorial port number 11. In our test, the total sample area is almost 10 times the area of the test chamber (0.49 m^2), which is in line with ITER recommendations for obtaining reliable data [12]. In fact, our vacuum test in the ITER database is the only one that meets this requirement.

IV. Evaluation of Gas Emission at the ITER EP #11

At the final design review (FDR) stage of EP #11, up to 60 B_4C blocks (Fig. 5) will be placed in each of the CuCrZr bronze trays (Fig. 6). The total number of trays estimated is 936 pieces [1]. The trays will fill all the free space in the diagnostic shield modules of the ports to improve neutron protection (Fig. 7). The design of the blocks was changed compared to the PDR stage, and the new design is shown in Fig. 5.

Each proposed boron carbide block has a surface area of 0.0122 m^2 and each tray has a B_4C surface area of 0.73 m^2, so the total area for the B_4C components per port will be 685 m^2 (the area is overestimated, as not all trays will contain 60 blocks, Fig. 7). The expected gas load at 100 °C at

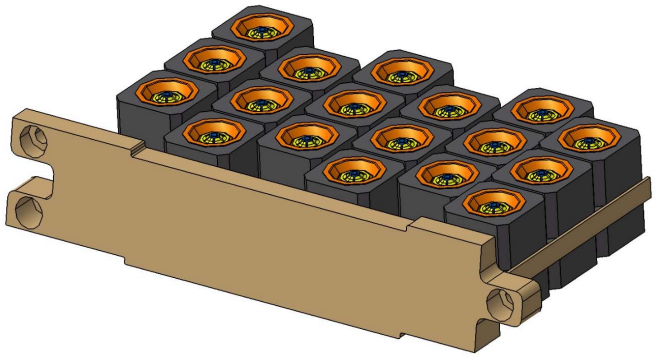

Fig. 6. CuCrZr bronze tray with B_4C blocks.

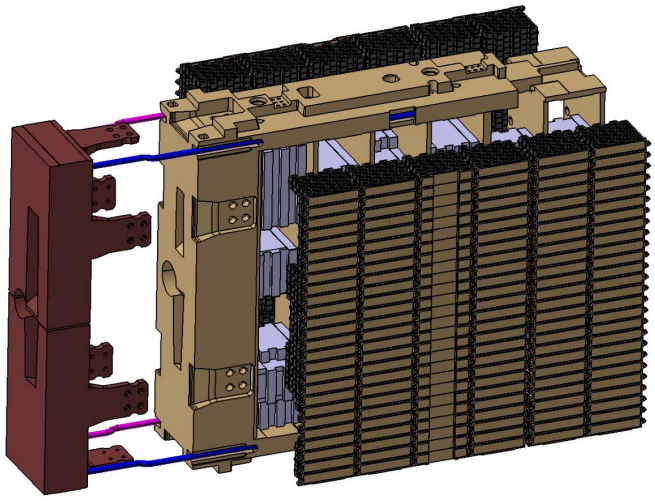

Fig. 7. ITER Equatorial port #11 Diagnostic Shield Module #2 with trays. All empty space is filled with ceramic trays.

TABLE II
Gas Load at 100 °C at the ITER EP #11

Material	Area [m^2]	Outgassing rate [$Pa \cdot m^3 \cdot s^{-1} \cdot m^{-2}$]	Outgassing load [$Pa \cdot m^3 \cdot s^{-1}$]
B_4C ceramics	685	1.0×10^{-8}	6.9×10^{-6}
Stainless steel	120	10^{-8}	1.2×10^{-6}
CuCrZr	210	1.3×10^{-8}	2.7×10^{-6}
Total	1015		1.1×10^{-5}

EP #11 for both types of Virial-made ceramics is calculated and shown in Table II.

The total area of EP #11 will be 1015 m^2, it will produce a gas load of $1.1 \cdot 10^{-5}$ $Pa \cdot m^3 \cdot s^{-1}$. If all eight equatorial diagnostic ports use a unified design and, accordingly, use boron carbide for neutron protection, the total gas flow from eight ports will be 8.8×10^{-5} $Pa \cdot m^3 \cdot s^{-1}$. On the basis of [12, paragraph 17.8.1, Appendix 17 IVH], an estimate of the gas budget for diagnostic ports was made, which was 10×10^{-5} $Pa \cdot m^3 \cdot s^{-1}$[1], [13]. Thus, the gas emission of diagnostic ports with ceramics does not exceed this limit and all ports can use boron carbide.

V. Study of Thermal Properties

The scheme of thermal conductivity measurements of the contact B_4C–CuCrZr bronze is presented in Fig. 8.

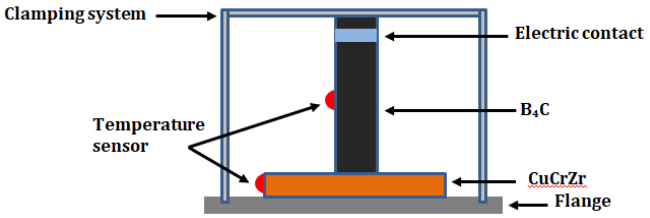

Fig. 8. Scheme of measurements of the thermal contact.

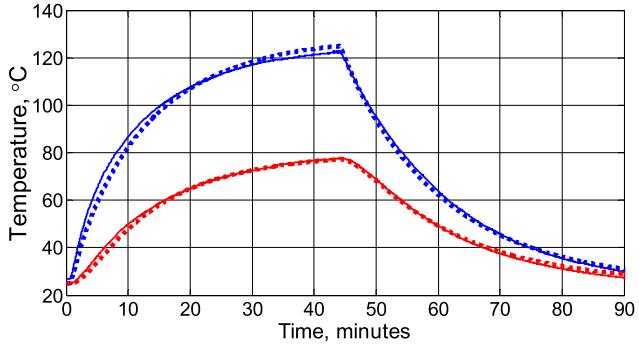

Fig. 9. Temperature dynamics. Blue: B_4C blocks. Red: bronze slab. Solid lines: measurements. Dots: discrete element simulation.

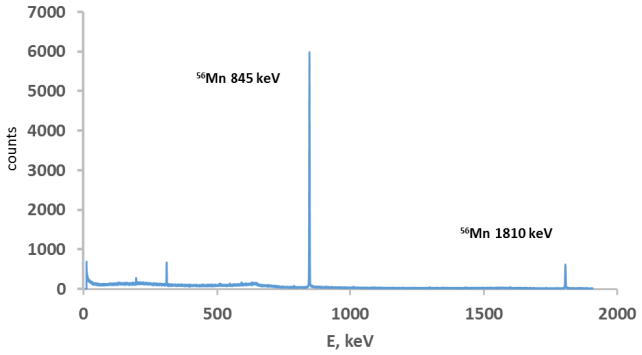

Fig. 10. Gamma radiation spectrum of SS 316L-IG after exposure to neutrons.

TABLE III
MANGANESE CONTENT MEASURED BY ACTIVATION METHOD

Ceramic	Mn content, %
Sintered, Virial	0.0001
Hotpressed, Virial	0.0002
Hotpressed, NEVZ	0.0001
Hotpressed, Beeforce	0.0003

The polished surface of the B_4C block was attached to the bronze plate surface. The surface roughness of B_4C and bronze was Ra 0.33 and Ra 1.4 micrometers, respectively, and the contact area was 13.1 cm^2. The reverse side of the bronze plate was connected to an air-cooled stainless steel (SS) flange. The assembly of the B_4C unit and the bronze plate was tightened using an initially calibrated spring with a tightening force of 1 MPa. The assembly was installed in a vacuum volume and pumped to a pressure of 10^{-1} Pa. The B_4C block was heated in volume by 3.9-A constant current using its own resistance to 120 °C temperature. The temperature was measured by thermoresistors glued to the B_4C block and the bronze plate with thermally conductive glue. The measured temperature dynamics of B4C is shown in Fig. 9 (solid lines). The results of measurements were compared with discrete element simulation of heat flow [14]. The measured value of the thermal conductivity of B_4C–CuCrZr contact was $6.3(+0.76, -2.3) \times 10^2$ W/(K·m^2). This value is several times lower than that measured in [15] [$\sim$3000 W/(K·m^2)]. Additional research is needed to clarify this issue.

Previously, data on the thermal conductivity of boron carbide were obtained: 20 W·m/K [1], which are in good agreement with the data on the reference material (10–28 W·m/K) [16].

VI. Activation of Ceramics by Low Energy Neutrons

When some atoms are irradiated with neutrons, nuclear reactions result in the appearance of radioactive isotopes. The decay of each isotope is specific and the energy of gamma rays identifies it [5]. Manganese isotopes were detected in the B_4C ceramic and SS 316L-ITER Grade (IG) (contains 1.83% Mn) spectra after irradiation with low energy neutrons. Neutrons were generated at an accelerator-based epithermal neutron source developed for boron neutron capture therapy of malignant tumors [6]. Gamma radiation spectrum of SS 316L-IG after exposure to neutrons is shown in Fig. 10. From the comparison of the gamma radiation intensity from the samples of ceramics of known mass and steel sample with known Mn content, the estimation of Mn content in ceramics is obtained (Table III). In the experiment, the irradiation time was 1 h and the neutron flux was 9×10^{12} neutrons/cm^2, which correspond well to the conditions for trays inside the Diagnostic Shield Module of EP #11 during the discharge of ITER. No cobalt decay lines were detected in the gamma radiation spectrum of ceramics.

VII. Conclusion

The amount of impurities in sintered and hot-pressed ceramics of boron carbide did not exceed 1%, which meets the requirements of ITER. Vacuum tests with large quantities of sintered boron carbide ceramics have shown that this type of ceramics can be used in ITER diagnostic ports to provide neutron protection (as well as hot-pressed ceramics). The measured thermal conductivity of ceramics was close to those expected. Contact thermal conductivity at the bronze boundary requires further study. Irradiation of ceramics by low energy neutrons has not revealed any dangerous impurities. All the above results, as well as the results of the neutron, mechanical, and thermohydraulic calculations of EP #11 with the boron carbide ceramic installed inside [17], were presented at the EP #11 FDR in July 2019. Thus, boron carbide ceramics can be used in the diagnostic ports of ITER.

REFERENCES

[1] A. Shoshin, A. Burdakov, M. Ivantsivskiy, M. Klimenko, S. Polosatkin, and A. Semenov, "Properties of boron carbide ceramics made by various methods for use in ITER," *Fusion Eng. Des.*, to be published. doi: 10.1016/j.fusengdes.2019.03.088.

[2] Y. A. Trunev *et al.*, "Heating of tungsten target by intense pulse electron beam," *AIP Conf. Proc.*, vol. 1771, Oct. 2016, Art. no. 060016. doi: 10.1063/1.4964224.

[3] A. A. Shoshin *et al.*, "Study of plasma-surface interaction at the GOL-3 facility," *Fusion Eng. Des.*, vol. 114, pp. 157–179, Jan. 2017. doi: 10.1016/j.fusengdes.2016.12.019.

[4] L. N. Vyacheslavov *et al.*, "Diagnostics of the dynamics of material damage by thermal shocks with the intensity possible in the ITER divertor," *Phys. Scripta*, vol. 93, Feb. 2018, Art. no. 035602. doi: 10.1088/1402-4896/aaa119.

[5] D. Kasatov, A. Makarov, I. Shchudlo, and S. Taskaev, "A study of gamma-ray and neutron radiation in the interaction of a 2 MeV proton beam with various materials," *Appl. Radiat. Isot.*, vol. 106, pp. 38–40, Dec. 2015. doi: 10.1016/j.apradiso.2015.08.011.

[6] S. Y. Taskaev *et al.*, "Accelerator based epithermal neutron source," *Phys. Part. Nuclei*, vol. 46, no. 6, pp. 956–990, Nov. 2015. doi: 10.1134/S1063779615060064.

[7] A. Badrutdinov *et al.*, "*In Situ* observations of blistering of a metal irradiated with 2-MeV protons," *Metals*, vol. 7, no. 12, p. 559, Dec. 2017. doi: 10.3390/met7120558.

[8] A. S. Arakcheev *et al.*, "Applications of synchrotron radiation scattering to studies of plasma facing components at siberian synchrotron and terahertz radiation centre," *AIP Conf. Proc.*, vol. 1771, Oct. 2016, Art. no. 060003. doi: 10.1063/1.4964211.

[9] A. S. Arakcheev *et al.*, "Dynamic observation of X-ray Laue diffraction on single-crystal tungsten during pulsed heat load," *J. Synchrotron Rad.*, vol. 26, no. 5, Sep. 2019. doi: 10.1107/S1600577519007306.

[10] A. S. Arakcheev *et al.*, "Theoretical investigation of crack formation in tungsten after heat loads," *J. Nucl. Mater.*, vol. 463, pp. 246–249, Aug. 2015. doi: 10.1016/j.jnucmat.2014.10.090.

[11] A. S. Arakcheev *et al.*, "Calculation of cracking under pulsed heat loads in tungsten manufactured according to ITER specifications," *J. Nucl. Mater.*, vol. 467, pp. 165–171, Dec. 2015. doi: 10.1016/j.jnucmat.2015.09.034.

[12] *ITER Vacuum Handbook*, ITER, Saint-Paul-lez-Durance, France, 2009, ITER_D_2EZ9UM.

[13] *55.QC Modular DSM Compatibility With IVH Outgassing Requirements*, ITER, Saint-Paul-lez-Durance, France, 2017, ITER_D_VXQAQM.

[14] *55. QB-R&D Report Thermal Conductibility of B4C/Bronze Border*, ITER, Saint-Paul-lez-Durance, France, 2019, ITER_D_YTX2R3.

[15] *Prototyping at CN DA (LEVI Harnessing, Shielding Blocks)*, ITER, Saint-Paul-lez-Durance, France, 2019, ITER_D_YPM8VR.

[16] G. S. Karumidze, L. I. Kekelidze, and L. A. Shengeliya, "Thermal conductivity of boron carbide as a function of ^{10}B content," *Semiconductors*, vol. 30, no. 10, pp. 921–923, Oct. 1996.

[17] Y. S. Sulyaev *et al.*, "Engineering calculations and preparation for manufacturing of ITER equatorial port #11," *IEEE Trans. Plasma Sci.*, to be published.